Journal Pre-proof

in-silico and *in-vitro* analysis of *IL36RN* mutations reveals critical residues for the function of the interleukin-36 receptor complex

Niina K. Hassi, Timir Weston, Giulia Rinaldi, Joseph C. Ng, Asma Smahi, Sophie Twelves, Camilla Davan-Wetton, Dana Fakhreddine, Franca Fraternali, Francesca Capon

PII: S0022-202X(23)02397-7

DOI: https://doi.org/10.1016/j.jid.2023.06.191

Reference: JID 3909

To appear in: *The Journal of Investigative Dermatology*

Received Date: 27 January 2023

Revised Date: 18 May 2023

Accepted Date: 8 June 2023

Please cite this article as: Hassi NK, Weston T, Rinaldi G, Ng JC, Smahi A, Twelves S, Davan-Wetton C, Fakhreddine D, Fraternali F, Capon F, *in-silico* and *in-vitro* analysis of *IL36RN* mutations reveals critical residues for the function of the interleukin-36 receptor complex, *The Journal of Investigative Dermatology* (2023), doi: https://doi.org/10.1016/j.jid.2023.06.191.

in-silico and *in-vitro* analysis of *IL36RN* mutations reveals critical residues for the function of the interleukin-36 receptor complex

Niina K Hassi[1], Timir Weston[2], Giulia Rinaldi[1], Joseph C Ng[2,4], Asma Smahi[3], Sophie Twelves[1], Camilla Davan-Wetton[1], Dana Fakhreddine[1], Franca Fraternali[2,4,5], Francesca Capon[1,5*]

[1]Department of Medical and Molecular Genetics and [2]Randall Centre for Cell and Molecular Biophysics, School of Basic and Medical Biosciences, King's College London, London, UK; [3]IMAGINE Institute INSERM UMR 1163, Paris, France; [4]Institute of Structural and Molecular Biology, University College London, London, UK. [5]These authors contributed equally.

*Correspondence to: Francesca Capon, 9th floor Tower Wing, Guy's Hospital, London SE1 9RT, UK; email: francesca.capon@kcl.ac.uk.

ORCIDs: Niina K Hassi, 0000-0002-1548-1199; Timir Weston, 0000-0002-9193-5578; Giulia Rinaldi, 0000-0002-4212-4584; Joseph C Ng, 0000-0002-3617-5211; Asma Smahi, 0000-0002-6002-0981; Sophie Twelves, 0000-0002-6568-2925; Camilla Davan-Wetton, 0000-0003-1252-7136; Dana Fakhreddine, 0000-0003-3521-7093; Franca Fraternali, 0000-0002-3143-6574; Francesca Capon, 0000-0003-2432-5793.

Running title: The structural impact of *IL36RN* mutations

Abbreviations: GERP, Genomic Evolutionary Rate Profiling; GPP, generalized pustular psoriasis; IL-36, interleukin-36; IL-36R, IL-36 receptor; IL-36Ra, IL-36 receptor antagonist.

ABSTRACT

Generalized pustular psoriasis (GPP) is a potentially life-threatening skin disease, associated with *IL36RN* mutations. *IL36RN* encodes the interleukin (IL)-36 receptor antagonist (IL-36Ra), a protein that downregulates the activity of IL-36 cytokines by blocking their receptor (IL-36R). While GPP can be treated with IL-36R inhibitors, the structural underpinnings of the IL-36Ra/IL-36R interaction remain poorly understood. Here, we sought to address this question by systematically investigating the effects of *IL36RN* mutations.

We experimentally characterized the effects of 30 *IL36RN* variants on protein stability. In parallel, we used a machine-learning tool (Rhapsody) to analyse the IL-36Ra three-dimensional structure and predict the impact of all possible amino acid substitutions. This integrated approach identified 21 amino acids that are essential to IL-36Ra stability.

We next investigated the effects of *IL36RN* changes on IL-36Ra/IL-36R binding and IL-36R signalling. By combining in-vitro assays and machine-learning with a second programme (mCSM), we identified 13 amino acids that are critical to IL-36Ra/IL36R engagement. Finally, we experimentally validated three representative predictions, further confirming the reliability of Rhapsody and mCSM.

These findings shed light on the structural determinants of IL-36Ra activity, with potential to facilitate the design of new IL-36 inhibitors and aid the interpretation of *IL36RN* variants in diagnostic settings.

INTRODUCTION

Interleukin (IL)-36α, IL36-β and IL36-γ are three IL-1 family cytokines that signal through a common receptor (IL-36R). Upon agonist binding, IL-36R associates with its accessory subunit (IL-1RacP), triggering a signalling cascade that culminates with the transcription of inflammatory genes such as *IL6* and *IL8* (Bassoy et al., 2018).

The activity of IL-36 cytokines is modulated by the IL-36 receptor antagonist (IL-36Ra). This protein also binds IL-36R, but prevents its association with IL-1RacP, thus inhibiting the activation of downstream pathways (Bassoyet al., 2018).

As IL-36 cytokines are mostly active at barrier sites (skin, gut, lung) effective IL-36Ra/IL-36R binding is critical for epithelial immune homeostasis (Han et al., 2020). In fact, loss-of-function mutations of the gene encoding IL-36Ra (*IL36RN*) are associated with generalized pustular psoriasis (GPP), a potentially life-threatening skin disorder presenting with recurrent pustular eruptions and systemic upset (Marrakchi et al., 2011, Onoufriadis et al., 2011).

The discovery of *IL36RN* mutations has informed the clinical development of a new class of biologics that restore skin immune homeostasis by blocking IL-36R activation (Macaes et al., 2022). Following two successful clinical trials (Bachelez et al., 2021, Bachelez et al., 2019), the anti-IL36R antibody spesolimab was granted FDA Breakthrough Therapy Designation, leading to its recent approval for the treatment of GPP (Blair, 2022). While spesolimab is also being investigated in hidradenitis suppurativa (Hwang et al., 2022) and atopic dermatitis (Bissonnette et al., 2022), other IL-36 inhibitors and approaches to IL-36 blockade are actively being researched (Zhukov et al., 2022) (Todorovic et al., 2019).

In this rapidly evolving landscape, a rigorous characterisation of *IL36RN* mutations could identify amino acid residues that are key to the function of the IL-36Ra/IL-36R complex, with the potential to inform further advances in drug design. The impact of *IL36RN* alleles, however, has not been fully investigated, with most functional studies focusing on two recurrent

mutations that are only observed in North-African (p.Leu27Pro) and European (p.Ser113Leu) populations (Marrakchiet al., 2011, Onoufriadiset al., 2011, Tauber et al., 2016). As the IL-36Ra structure has not been experimentally resolved, studies of variant effects have also been hindered by an incomplete understanding of the protein three-dimensional conformation.

Here we have addressed this issue by exploiting the seminal work of the DeepMind AlphaFold2 project, which has recently inferred >200M highly accurate protein structures (Jumper et al., 2021, Varadi et al., 2022). By combining the computational analysis of AlphaFold2 structures with the experimental characterization of mutant constructs, we have systematically assessed the effects of *IL36RN* sequence changes. This integrated approach has enabled us to identify key residues that are essential to IL-36Ra stability and IL-36Ra/IL-36R binding.

RESULTS

Variant selection

To explore the impact of missense alleles on IL-36Ra function, we examined 30 variants distributed along the entire protein sequence (Figure 1a). These included 17 rare changes observed in GPP cases (patient variants, Table S1), 12 rare changes randomly selected from dbSNP database (population variants, Table S2) and one common change detected in >10% of East Asians (p.Asn47Ser).

Variant effects on protein stability

We first investigated the effect of *IL36RN* variants on protein folding and stability. We generated mutagenized constructs for the 30 selected changes and over-expressed each cDNA in HeLa cells. We then measured protein accumulation by western blotting.

These experiments confirmed that p.Pro27Leu and p.Ser113Leu alleles, previously characterised as destabilising mutations (Marrakchiet al., 2011, Onoufriadiset al., 2011), were

associated with a marked reduction in IL-36Ra levels (>4-fold decrease in protein accumulation compared to wild-type construct). A similar effect was observed for three additional GPP alleles (p.Ile42Asn, p.Glu112Lys, p.Thr123Arg) (Figure 1B and 1C).

The five residues affected by the destabilising changes were under strong evolutionary constraint, showing higher Genomic Evolutionary Rate Profiling (GERP) scores (Davydov et al., 2010) than the population variants (average GERP score: 1.69 vs -0.3; *P*=0.038). While four of the five (80%) changes mapped to beta-sheets within the protein core (Figure 2), only one of 13 population variants (7.7%) was found in a similar location (*P*=0.008; Fisher's exact test).

Only one population variant (p.Cys70Arg) had destabilising effects. Interestingly, the amino acid affected by this change forms a hydrogen bond with Ser113, the target of the recurrent p.Ser113Leu mutation (Figure 2). Thus, the Ser113/Cys70 interaction is likely to be important for stable IL-36Ra folding.

To further explore these findings, we assessed the effect of destabilising mutations using Rapid High-Accuracy Prediction of SAV Outcome based on DYnamics (Rhapsody). This is a machine learning tool that predicts variant pathogenicity by considering structural features and intrinsic protein dynamics (e.g., local fluctuations in residue position) (Ponzoni et al., 2020). Here, we used Rhapsody to analyse the IL-36Ra structure generated by DeepMind AlphaFold2. We found that all destabilising changes were associated with high (>50%) likelihoods of pathogenicity (Table S1). We also observed an overall correlation between Rhapsody scores and experimental measurement of protein stability (r=-0.63; *P*=0.0003) (Figure 3A).

Interestingly, sequence-based pathogenicity predictors did not perform as well. CADD (Rentzsch et al., 2019) classified most changes (25/30) as pathogenic, including the common p.Asn47Ser variant. REVEL (Ioannidis et al., 2016), which has been described as an accurate variant effect predictor for autoinflammatory mutations (Accetturo et al., 2020), offered better

discrimination between benign and damaging alleles (Figure S1). However, it misclassified the best characterised *IL36RN* mutation (p.Ser113Leu) (Onoufriadiset al., 2011, Tauberet al., 2016) as "likely benign".

Saturation mutagenesis identifies variants that are essential to IL-36Ra stability

Having established that Rhapsody is the tool that best recapitulates the effects of *IL36RN* variants on protein stability, we decided to use this program for *in-silico* saturation mutagenesis. We simulated all possible amino acid substitutions for each of the 155 residues that form the IL-36Ra protein. We then calculated pathogenicity scores for each change (Figure 3B). This confirmed the pattern observed in our stability assays, demonstrating that the 15 IL-36Ra residues that are most intolerant to mutations (top decile, Table S3) are more likely to map to β-strands than the remaining amino acids (80.0% vs 47.8%, P=0.027). These residues are also less accessible to solvents than the rest of the amino acids (average fraction of solvent accessible surface area (QSASA): 0.21 vs 0.38, P=0.023), indicating a preferential localization within the protein core. In fact, eight of the top decile residues cluster to three spatially adjacent β-sheets spanning amino acids 56-61, 96-104 and 119-123 (Table S3). Thus, the combination of *in-vitro* and *in-silico* methods has allowed us to identify key residues that are critical to the folding and stability of IL-36Ra.

Variant effects on receptor binding affinity

The majority of disease alleles that do not affect protein folding disrupt protein-protein interactions (Sahni et al., 2015). We therefore hypothesised that *IL36RN* mutations mapping to the protein surface would destabilise the engagement of IL-36Ra with its receptor, favouring IL-36/IL-36R signalling over IL-36Ra/IL-36R binding. To validate this hypothesis, we treated HeLa cells with wild-type or mutant IL-36Ra, before stimulating the cultures with IL-36α. We

then measured the production of IL-8 (Figure S2). We selected this chemokine as a readout of IL-36/IL-36R signalling because it is potently induced by all IL-36 cytokines (Mahil et al., 2017, Swindell et al., 2018) and is markedly overexpressed in GPP skin (Baum et al., 2022). IL-8 is also downregulated following disease treatment with spesolimab or retinoids (Baumet al., 2022, Wang et al., 2018) (Table S4). In fact, IL-8 plays a key role in driving neutrophilic inflammation (Matsushima et al., 2022), so that its induction has been the focus of various studies characterising the effects of *IL36RN* mutations (Bal et al., 2019, Marrakchiet al., 2011, Tauberet al., 2016).

Here, we measured IL-36 dependent IL-8 production to analyse the effects of 14 IL-36Ra surface changes (10 patient and 4 population variants) that did not destabilise the protein structure. We found that most patient alleles led to the upregulation of IL-36 signalling, whereas population variants did not (Figure 4A). In fact, the average IL8-fold induction was 2.25 for patient alleles vs 1.48 for population variants (P=5.3 x10^{-5}).

The results of the activity assays did not correlate with the output of sequence-based pathogenicity predictors (CADD and REVEL) or GERP scores (P>0.2 for all). As Rhapsody has been developed for the analysis of single proteins, we sought an alternative, structure-based approach, allowing us to model the effect of amino acid substitutions on the IL-36Ra/IL-36R interaction.

We first used protein-protein docking to model the structure of the IL-36Ra/IL-36R complex, based on that of its constituent proteins. We then analysed the impact of *IL36RN* sequence variants using mCSM and mCSM-PPI2, two machine learning tools that predicts the effects of missense changes on protein binding affinity (Pires et al., 2014, Rodrigues et al., 2019). This analysis showed that the impact of *IL36RN* alleles predicted by mCSM (the change in Gibbs free energy or ΔΔG) is significantly correlated with their effect on IL-36 activity (r = -0.53, P= 0.045) (Figure 4B).

Having established the reliability of its predictions, we used mCSM to systematically investigate which IL-36Ra residues can be mutated without affecting receptor-ligand interactions. We undertook computational alanine scanning, a process whereby the amino acids of a target protein are substituted with Ala to eliminate side-chain interactions while preserving the native structure of the protein. This showed that 91% of residue changes had a mild ($-1<\Delta\Delta G<0$) or moderate ($-2<\Delta\Delta G<-1$) de-stabilising effect on the IL-36R/IL-36Ra interaction (Figure 4C). Interestingly, the 15 amino acids that are most intolerant to substitutions (top decile, Table S3) include the residues that are affected by the p.His32Arg, p.Arg48Trp, p.Pro76Leu, p.Arg102Trp and p.Glu112Lys mutations. These residues were more frequently found on the IL-36Ra/IL-36R binding interface than the remaining IL-36Ra amino acids (46.7% vs 19.2%, P=0.023).

Validation of in-silico predictions

Our correlation analyses suggest that protein stability is most accurately predicted with Rhapsody, while mCSM is the best tool to assess the impact of amino acid substitutions on IL-36Ra/IL-36R binding affinity.

To further confirm this, we selected representative predictions for experimental validation. We focused on three changes that are reported as variants of unknown significance in the ClinVar database of genomic variation: p.Cys67Phe (affecting a beta-helix in the protein core), p.Ala92Val (affecting a surface residue that does not map to the receptor binding interface) and p.Gln129Arg (affecting a surface residue that maps to the receptor binding interface).

Rhapsody predicts a deleterious effect for p.Cys67Phe (pathogenicity probability: 0.77), but not p.Ala92Val or p.Gln129Arg (pathogenicity probabilities: 0.12 and 0.34, respectively). Accordingly, western blot analysis showed a reduction in protein accumulation for the p.Cys67Phe protein but not the p.Ala92Val and p.Gln129Arg mutants (Figure 5A).

mCSM scores suggested that the effect of p.Ala92Val was modest (ΔΔG= -0.38 kcal/mol) and that p.Gln129Arg was mildly destabilising (ΔΔG= -0.65 kcal/mol). These predictions were experimentally verified, as our activity assay showed that p.Gln129Arg, but not Ala92Val, had an impact on IL-36 signalling (Figure 5B).

DISCUSSION

The aim of our study was to characterize the IL-36Ra residues that are essential to the stability of the protein and its interaction with IL-36R. We combined experimental and computational approaches, using the former to validate the performance of two well established predictors of variant impact: Rhapsody for single molecule stability and mCSM for protein-protein interaction. We then used these tools to systematically investigate the IL-36Ra structure generated by the AlphaFold2 artificial intelligence system.

Of note, a recent community assessment confirmed that pathogenicity predictions based on AlphaFold2 models were as accurate as those relying on experimental structures. AlphaFold2 models also performed better than homology-based ones, especially when the latter were derived from distantly related templates (Akdel et al., 2022).

Importantly, confidence metrics associated with individual amino acids were identified as an important parameter influencing the accuracy of variant effect prediction (Akdelet al., 2022). This validates our decision to use AlphaFold2 models for IL-36Ra (<5% of residues predicted with low confidence) but not IL-36R (>15% of residues predicted with low or very low confidence).

Recent studies also showed that the AlphaFold2 system cannot directly infer the impact of amino acid changes on protein structure (Buel and Walters, 2022, Pak et al., 2021), supporting our strategy of using tools specifically designed for pathogenicity predictions. We specifically

selected Rhapsody and mCSM, based on significant correlations with our experimental results and high performance with benchmark datasets (Pireset al., 2014, Ponzoniet al., 2020).

In keeping with experimental results obtained in other systematic studies of variant effects (Hoie et al., 2022), our Rhapsody analysis demonstrated that the amino acids that are essential to protein stability are mostly buried in the core. In this case, the observation is particularly noteworthy as IL-36Ra is a low molecular weight protein (17 kDa) with a small hydrophobic core. In this context, the p.Cys67Phe substitution examined in our validation experiment had a destabilising effect. While this change was identified in a single GPP patient (Zea-Vera et al., 2019) and is currently classified as a variant of unknown significance, our computational and experimental findings indicate that it could be considered as a pathogenic mutation. Conversely, the p.Ala92Val and p.Gln129Arg surface substitutions are likely to be benign, as mCSM scores and IL-36 activity assays point to very modest effects on receptor binding affinity. Thus, our observations support the application of Rhapsody and mCSM for the interpretation of *IL36RN* variants. Given that these tools outperformed sequence-based predictors in our analyses, their application could be particularly informative in diagnostic settings, where *IL36RN* is often sequenced as part of an autoinflammatory disease gene panel (Omoyinmi et al., 2017).

In our study, we also used Rhapsody for *in silico* saturation mutagenesis and mCSM for Alanine scanning. The former analysis uncovered clusters of hydrophobic residues (e.g., Phe98/Phe100; Pro117/Trp119/Leu121) that are essential to IL-36Ra folding and stability. These amino acids are that likely to play an important role in maintaining the structure of IL-1 family cytokines, as they are broadly conserved in paralogue proteins, such as IL-1Ra, IL-36α, IL-36γ and IL-38 (Wang et al., 2010). The latter cytokine is of particular interest, given it can bind IL-36R and inhibit downstream signalling, similarly to IL-36Ra (de Graaf et al., 2022).

Alanine scanning identified key hydrophilic amino acids (e.g., His22, Asn23, Arg102) at the IL-36Ra/IL-36R binding interface. Of note, none of these residues are conserved in IL-38, even if their hydrophilic properties are preserved (the corresponding positions are: Arg23, Asp24, Gln103) (de Graafet al., 2022). In this context, our integrated *in-vitro/in-silico* approach could be applied to the study of IL-36R/IL-38 binding, with the potential to reveal the structural determinants of its inhibitory function. Given the IL-38 signalling complex has yet to be crystalized, such studies could prove particularly informative.

While the effects of IL-36Ra have been more extensively investigated than those of IL-38 (Bassoyet al., 2018), the only experimentally resolved structure for IL-36R is that of the extracellular domain of the receptor, in complex with a spesolimab fragment (Larson et al., 2020). Thus, our dissection of IL-36Ra/IL-36R binding sheds light on the structural determinants of this interaction, with the potential to facilitate the design of novel IL-36 inhibitors for the treatment of skin inflammation.

METHODS

IL-36Ra protein structure

The IL-36Ra protein structure generated by AlphaFold2 (Varadiet al., 2022) (AF-Q9UBH0-F1-model_v3.pdb) was obtained from the AlphaFold Protein Structure Database at https://alphafold.ebi.ac.uk. Predicted local-distance difference test (pLDDT) scores were also retrieved, confirming that only 5 of 155 residue positions (3%) had been inferred with low confidence (50<pLDDT<70). The structure was validated with MolProbity (Williams et al., 2018) (http://molprobity.biochem.duke.edu/).

Modelling of the IL-36Ra/IL-36R complex

The AlphaFold2 IL-36R structure (AF-Q9HB29-F1-model_v3.pdb) was deemed unsuitable for analysis as >15% of residue positions had been inferred with low or very-low (pLDDT<50) confidence. The three-dimensional structure of IL-36R was therefore derived by homology modelling. The IL-36R amino acid sequence (UniProt ID: Q9HB29) was used to search the Protein Data Bank (PDB, www.rcsb.org), using the Basic Local Alignment Search Tool (Altschul et al., 1990) (BLAST, https://blast.ncbi.nlm.nih.gov/Blast.cgi). The top hit (IL-1/IL-1Ra complex; PDB entry 1IRA) was aligned with IL-36Ra using T-Coffee (Notredame et al., 2000). The three-dimensional protein structure was then predicted with SWISS-MODEL (Waterhouse et al., 2018) and validated with MolProbity.

Next, three-dimensional models of IL-36Ra and IL-36R were aligned to the experimentally resolved structure of the IL-1/IL-1Ra complex (PDB ID: 1IRA), using PyMol (Schrodinger, New York, NY). RosettaDock (Chaudhury et al., 2011) (https://r2.graylab.jhu.edu) was then used to infer the most energetically favourable model for the IL-36Ra-IL-36R complex. The predicted IL36-Ra/IL36R structure with the lowest interface energy score, overall root-mean-squared deviation (RMSD) and interface RMSD was selected for analysis with the tools listed below.

The programs mCSM (Pireset al., 2014) (http://biosig.unimelb.edu.au/mcsm/) and mCSM-PPI2 (Rodrigueset al., 2019) (https://biosig.lab.uq.edu.au/mcsm_ppi2/) were used to quantify the changes to a calculated score that is a proxy to the Gibb's free energy (ΔΔG) associated with each variant. The fraction of solvent accessible surface area (QSASA, equal to the quotient between solvent accessible surface and total surface) was calculated for each residue, using POPScomp (Fraternali and Cavallo, 2002) (http://popscomp.org:3838/). Amino acids mapping to the IL-36R/IL36Ra binding interface were identified with MutaBind2 (Zhang et al., 2020) (https://lilab.jysw.suda.edu.cn/research/mutabind2/).

IL-36Ra stability assay

For protein stability assays, HeLa-IL36R cells were transfected with wild-type or mutant myc-IL36RN, using Lipofectamine 2000 (Life Technologies, Carlsbad, CA; catalogue n: 11668027). Transfected HeLa-IL36R cells were harvested after 18hr, and protein extracts were analyzed by western blotting, as described in the Supplementary Methods.

IL-36Ra activity assay

IL-36Ra proteins used in activity assays were generated by transfecting HEK293 cells with wild-type or mutant myc-IL36RN, using Lipofectamine 2000. After 24hr, cells were harvested and recombinant proteins were isolated from lysates, using the c-Myc tagged protein mild purification kit (MBL International Corporation, Woburn, MA; catalogue n:3305).

HeLa-IL36R cells were first starved in supplement-free RPMI for 4hr and then treated with 300ng purified IL-36Ra protein (wild-type or mutant, generated as described above). After 30 minutes, cultures were stimulated with 10ng/ml IL36α (RD Systems, Minneapolis, MN; catalogue n: 6995-IL). Culture supernatants were collected after 4 hours and analysed by ELISA.

Statistics

Correlation analyses were implemented with Spearman rank test. The characteristics of IL-36Ra proteins harbouring different changes (wild-type vs mutant sequence, population vs patient variant) were compared using an unpaired t-test or Fisher's exact test, as appropriate. All tests were implemented in R v4.1.1.

DATA AVAILABILITY STATEMENT: The authors confirm that the data supporting the findings of this study are available in the article and its Supplementary Materials.

CONFLICT OF INTERESTS: FC has received research grants and consultancy fees from Boehringer Ingelheim.

ACKNOWLEDGEMENTS

We are very grateful to Claire Peet and Luc Francis for their assistance. This research was supported by the National Institute for Health and Care Research (NIHR) Biomedical Research Centre based at Guy's and St Thomas' NHS Foundation Trust and King's College London (guysbrc-2012-1). We also received funding from the Medical Research Council, the Biotechnology and Biological Sciences Research Council (BBSRC) (grants MR/L01257X/2 and BB/T002212/1 to FF) and the British Skin Foundation (grant 008S/22 to FC and FF). ST was supported by the King's Bioscience Institute and the Guy's and St Thomas' Charity Prize PhD Programme in Biomedical and Translational Science. CDW and DF were funded by the BBSRC through the London Interdisciplinary Doctoral Training Partnership (LIDo-DTP) [grants BB/M009513/1 and BB/T008709/1].

The views expressed are those of the author(s) and not necessarily those of the NHS, the NIHR or the Department of Health and Social Care. None of the funders was involved in the study design, data collection, data analysis or manuscript preparation.

AUTHOR CONTRIBUTIONS

Conceptualization: FC, FF; Formal analysis: GR, JCN, TW; Funding acquisition: FC, FF; Investigation: CDW, DF, NKH, ST; Resources: AS; Supervision: FC, FF; Writing-review & editing: FC, FF, GR, JCN, TW; Writing-original draft preparation: FC.

REFERENCES

Accetturo M, D'Uggento AM, Portincasa P, Stella A. Improvement of MEFV gene variants classification to aid treatment decision making in familial Mediterranean fever. Rheumatology 2020;59(4):754-61.

Akdel M, Pires DEV, Pardo EP, Janes J, Zalevsky AO, Meszaros B, et al. A structural biology community assessment of AlphaFold2 applications. Nat Struct Mol Biol 2022;29(11):1056-67.

Altschul SF, Gish W, Miller W, Myers EW, Lipman DJ. Basic local alignment search tool. Journal of molecular biology 1990;215(3):403-10.

Bachelez H, Choon SE, Marrakchi S, Burden AD, Tsai TF, Morita A, et al. Trial of Spesolimab for Generalized Pustular Psoriasis. N Engl J Med 2021;385(26):2431-40.

Bachelez H, Choon SE, Marrakchi S, Burden AD, Tsai TF, Morita A, et al. Inhibition of the Interleukin-36 Pathway for the Treatment of Generalized Pustular Psoriasis. N Engl J Med 2019;380(10):981-3.

Bal E, Lim AC, Shen M, Douangpanya J, Madrange M, Gazah R, et al. Mutation in IL36RN impairs the processing and regulatory function of the interleukin-36-receptor antagonist and is associated with DITRA syndrome. Exp Dermatol 2019;28(10):1114-7.

Bassoy EY, Towne JE, Gabay C. Regulation and function of interleukin-36 cytokines. Immunological reviews 2018;281(1):169-78.

Baum P, Visvanathan S, Garcet S, Roy J, Schmid R, Bossert S, et al. Pustular psoriasis: Molecular pathways and effects of spesolimab in generalized pustular psoriasis. The Journal of allergy and clinical immunology 2022;149(4):1402-12.

Bissonnette R, Abramovits W, Saint-Cyr Proulx E, Lee P, Guttman-Yassky E, Zovko E, et al. Spesolimab, an anti-interleukin-36 receptor antibody, in patients with moderate-to-severe atopic dermatitis: results from a multicenter, randomized, double-blind, placebo-controlled,

phase IIa study. Journal of the European Academy of Dermatology and Venereology : JEADV 2022.

Blair HA. Spesolimab: First Approval. Drugs 2022;82(17):1681-6.

Buel GR, Walters KJ. Can AlphaFold2 predict the impact of missense mutations on structure? Nat Struct Mol Biol 2022;29(1):1-2.

Chaudhury S, Berrondo M, Weitzner BD, Muthu P, Bergman H, Gray JJ. Benchmarking and analysis of protein docking performance in Rosetta v3.2. PLoS One 2011;6(8):e22477.

Davydov EV, Goode DL, Sirota M, Cooper GM, Sidow A, Batzoglou S. Identifying a high fraction of the human genome to be under selective constraint using GERP++. PLoS Comput Biol 2010;6(12):e1001025.

de Graaf DM, Teufel LU, Joosten LAB, Dinarello CA. Interleukin-38 in Health and Disease. Cytokine 2022;152:155824.

Fraternali F, Cavallo L. Parameter optimized surfaces (POPS): analysis of key interactions and conformational changes in the ribosome. Nucleic acids research 2002;30(13):2950-60.

Han Y, Huard A, Mora J, da Silva P, Brune B, Weigert A. IL-36 family cytokines in protective versus destructive inflammation. Cell Signal 2020;75:109773.

Hoie MH, Cagiada M, Beck Frederiksen AH, Stein A, Lindorff-Larsen K. Predicting and interpreting large-scale mutagenesis data using analyses of protein stability and conservation. Cell reports 2022;38(2):110207.

Hwang J, Rick J, Hsiao J, Shi VY. A review of IL-36: an emerging therapeutic target for inflammatory dermatoses. The Journal of dermatological treatment 2022;33(6):2711-22.

Ioannidis NM, Rothstein JH, Pejaver V, Middha S, McDonnell SK, Baheti S, et al. REVEL: An Ensemble Method for Predicting the Pathogenicity of Rare Missense Variants. Am J Hum Genet 2016;99(4):877-85.

Jumper J, Evans R, Pritzel A, Green T, Figurnov M, Ronneberger O, et al. Highly accurate protein structure prediction with AlphaFold. Nature 2021;596(7873):583-9.

Larson ET, Brennan DL, Hickey ER, Ganesan R, Kroe-Barrett R, Farrow NA. X-ray crystal structure localizes the mechanism of inhibition of an IL-36R antagonist monoclonal antibody to interaction with Ig1 and Ig2 extra cellular domains. Protein science : a publication of the Protein Society 2020;29(7):1679-86.

Macaes CO, Le AM, Torres T. Generalized pustular psoriasis: the new era of treatment with IL-36 receptor inhibitors. The Journal of dermatological treatment 2022;33(7):2911-8.

Mahil SK, Catapano M, Di Meglio P, Dand N, Ahlfors H, Carr IM, et al. An analysis of IL-36 signature genes and individuals with IL1RL2 knockout mutations validates IL-36 as a psoriasis therapeutic target Science translational medicine 2017;9:eaan2514.

Marrakchi S, Guigue P, Renshaw BR, Puel A, Pei XY, Fraitag S, et al. Interleukin-36-receptor antagonist deficiency and generalized pustular psoriasis. N Engl J Med 2011;365(7):620-8.

Matsushima K, Yang D, Oppenheim JJ. Interleukin-8: An evolving chemokine. Cytokine 2022;153:155828.

Notredame C, Higgins DG, Heringa J. T-Coffee: A novel method for fast and accurate multiple sequence alignment. Journal of molecular biology 2000;302(1):205-17.

Omoyinmi E, Standing A, Keylock A, Price-Kuehne F, Melo Gomes S, Rowczenio D, et al. Clinical impact of a targeted next-generation sequencing gene panel for autoinflammation and vasculitis. PLoS One 2017;12(7):e0181874.

Onoufriadis A, Simpson MA, Pink AE, Di Meglio P, Smith CH, Pullabhatla V, et al. Mutations in IL36RN/IL1F5 are associated with the severe episodic inflammatory skin disease known as generalized pustular psoriasis. Am J Hum Genet 2011;89(3):432-7.

Pak MA, Markhieva KA, Novikova MS, Petrov DS, Vorobyev IS, Maksimova ES, et al. Using AlphaFold to predict the impact of single mutations on protein stability and function. BioRxiv 2021.

Pires DE, Ascher DB, Blundell TL. mCSM: predicting the effects of mutations in proteins using graph-based signatures. Bioinformatics 2014;30(3):335-42.

Ponzoni L, Penaherrera DA, Oltvai ZN, Bahar I. Rhapsody: predicting the pathogenicity of human missense variants. Bioinformatics 2020;36(10):3084-92.

Rentzsch P, Witten D, Cooper GM, Shendure J, Kircher M. CADD: predicting the deleteriousness of variants throughout the human genome. Nucleic acids research 2019;47(D1):D886-D94.

Rodrigues CHM, Myung Y, Pires DEV, Ascher DB. mCSM-PPI2: predicting the effects of mutations on protein-protein interactions. Nucleic acids research 2019;47(W1):W338-W44.

Sahni N, Yi S, Taipale M, Fuxman Bass JI, Coulombe-Huntington J, Yang F, et al. Widespread macromolecular interaction perturbations in human genetic disorders. Cell 2015;161(3):647-60.

Swindell WR, Beamer MA, Sarkar MK, Loftus S, Fullmer J, Xing X, et al. RNA-Seq Analysis of IL-1B and IL-36 Responses in Epidermal Keratinocytes Identifies a Shared MyD88-Dependent Gene Signature. Frontiers in immunology 2018;9:80.

Tauber M, Bal E, Pei XY, Madrange M, Khelil A, Sahel H, et al. IL36RN Mutations Affect Protein Expression and Function: A Basis for Genotype-Phenotype Correlation in Pustular Diseases. J Invest Dermatol 2016;136(9):1811-9.

Todorovic V, Su Z, Putman CB, Kakavas SJ, Salte KM, McDonald HA, et al. Small Molecule IL-36gamma Antagonist as a Novel Therapeutic Approach for Plaque Psoriasis. Scientific reports 2019;9(1):9089.

Varadi M, Anyango S, Deshpande M, Nair S, Natassia C, Yordanova G, et al. AlphaFold Protein Structure Database: massively expanding the structural coverage of protein-sequence space with high-accuracy models. Nucleic acids research 2022;50(D1):D439-D44.

Wang D, Zhang S, Li L, Liu X, Mei K, Wang X. Structural insights into the assembly and activation of IL-1beta with its receptors. Nat Immunol 2010;11(10):905-11.

Wang L, Yu X, Wu C, Zhu T, Wang W, Zheng X, et al. RNA sequencing-based longitudinal transcriptomic profiling gives novel insights into the disease mechanism of generalized pustular psoriasis. BMC Med Genomics 2018;11(1):52.

Waterhouse A, Bertoni M, Bienert S, Studer G, Tauriello G, Gumienny R, et al. SWISS-MODEL: homology modelling of protein structures and complexes. Nucleic acids research 2018;46(W1):W296-W303.

Williams CJ, Headd JJ, Moriarty NW, Prisant MG, Videau LL, Deis LN, et al. MolProbity: More and better reference data for improved all-atom structure validation. Protein science : a publication of the Protein Society 2018;27(1):293-315.

Zea-Vera AF, Estupinan-Lopez FE, Cifuentes-Burbano J, Vargas MJ, Bonelo A. Interleukin-36 Receptor Antagonist Deficiency (DITRA) with a Novel IL36RN Homozygous Mutation c.200G > T (P.Cys67Phe) in a Young Colombian Woman. Journal of clinical immunology 2019;39(3):261-3.

Zhang N, Chen Y, Lu H, Zhao F, Alvarez RV, Goncearenco A, et al. MutaBind2: Predicting the Impacts of Single and Multiple Mutations on Protein-Protein Interactions. iScience 2020;23(3):100939.

Zhukov AS, Khairutdinov VR, Samtsov AV, Krasavin M, Garabadzhiu AV. Preclinical efficacy investigation of human neutrophil elastase inhibitor sivelestat in animal model of psoriasis. Skin Health Dis 2022;2(2):e90.

FIGURE LEGENDS

Figure 1: **Effects of *IL36RN* sequence variants on protein stability**. **a)** Schematic showing the position of the examined variants. Changes observed in affected individuals are highlighted in red, with the recurrent p.Pro27Leu and p.Ser113Leu mutations in underlined font. The common p.Asn47Ser variant is shown in green, while rare population variants from the gnomAD database are in black. **b)** Representative western blots showing the accumulation of wild-type (WT) and mutant IL-36Ra, following the transfection of the relevant cDNA constructs into HeLa cells. **c)** Densitometry results for patient (left) and population (right) variants. Stability was calculated as the IL-36Ra/β-actin ratio normalised to wild-type values. Results are presented as means +/- standard deviation for 3 independent transfections. **P*<0.05; ***P*<0.01; ****P*<0.001.

Figure 2: **Mapping destabilising changes to the three-dimensional IL-36Ra structure**. Each panel shows the position of the residues impacted by mutations (left) with the enlarged view (right) displaying the hydrogen bonds formed with neighbouring amino acids (blue dotted lines on structures). All residues except Thr123 map to beta strands (blue ribbons) within the protein core.

Figure 3: **Rhapsody pathogenicity predictions**. **a)** Pathogenicity probabilities calculated by Rhapsody (Rhapsody scores) demonstrate a significant correlation with experimental measurements of protein stability (calculated as in 1C). Destabilising mutations generating high Rhapsody scores are highlighted with a red circle. **b)** Heatmap illustrating the results of in-silico saturation mutagenesis. Each column shows the Rhapsody pathogenicity probabilities for all possible substitutions at a given residue. The series of dark green squares above the

diagram represents the IL36Ra amino acid sequence, with α-helixes and β-strands highlighted by coloured bars.

Figure 4: Effects of *IL36RN* sequence variants on receptor binding affinity a) Bar plot showing the effects of patient (left) and population (right) variants on IL-36 signalling (measured as IL-36 induced IL-8 production, normalised to wild-type). All results are presented as means +/- standard deviation for 3 independent transfections.*P<0.05 and **P<0.01 for variants associated with at least 2-fold increase in IL-36 activity; **b)** Changes in receptor binding affinity calculated by mCSM (ΔΔG values) demonstrate a significant correlation with experimental measurements of IL-36 signalling. **c)** Heatmap illustrating the results of Ala scanning mutagenesis. Each cell shows the mCSM ΔΔG values for the relevant residue.

Figure 5: Validation of bioinformatic predictions for selected changes a) Left: representative western blot showing the accumulation of wild-type (WT) and mutant IL-36Ra, following the transfection of the relevant cDNA constructs into HeLa cells. The p.Pro27Leu mutation was analysed as a positive control and is highlighted in red underlined font Right: Densitometry results. Stability was calculated as the IL-36Ra/β-actin ratio normalised to wild-type. **b)** Bar plot showing the effects of selected variants on IL-36 signalling activity. All results are presented as means +/- standard deviation for 3 independent transfections.*P<0.05; **P<0.01; ***P<0.001.

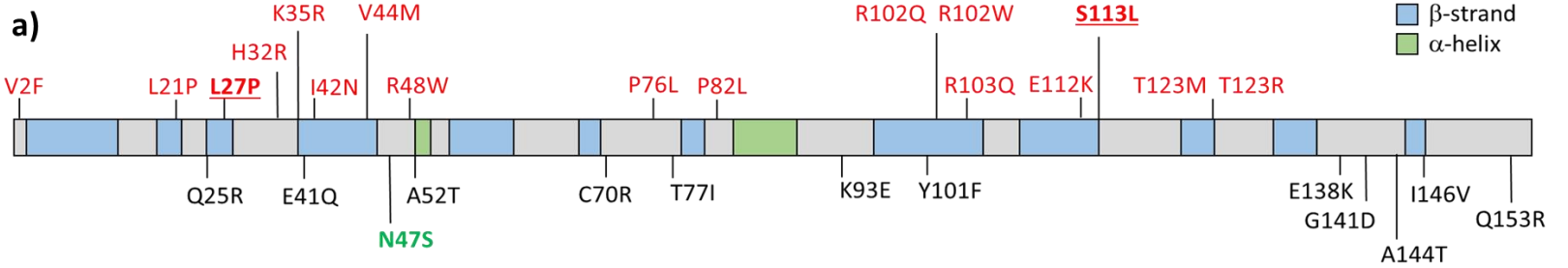

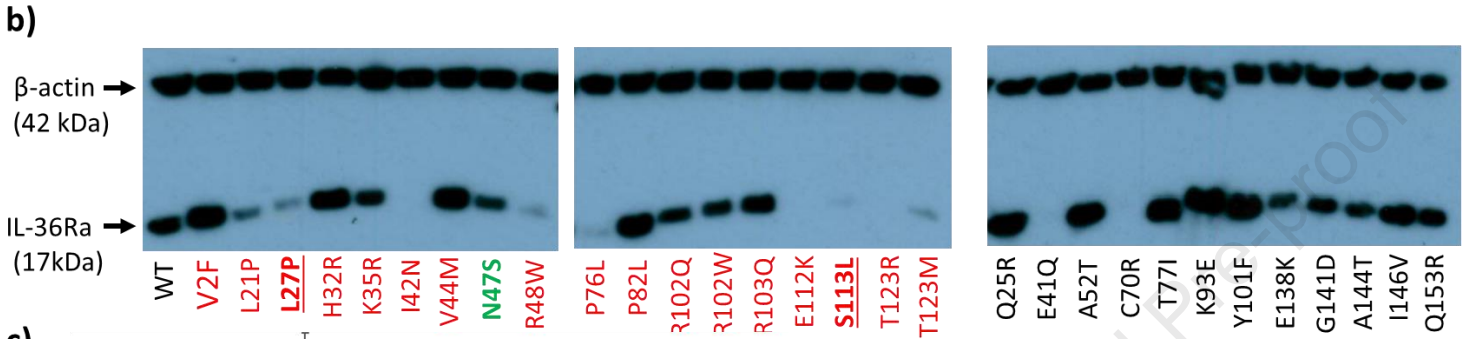

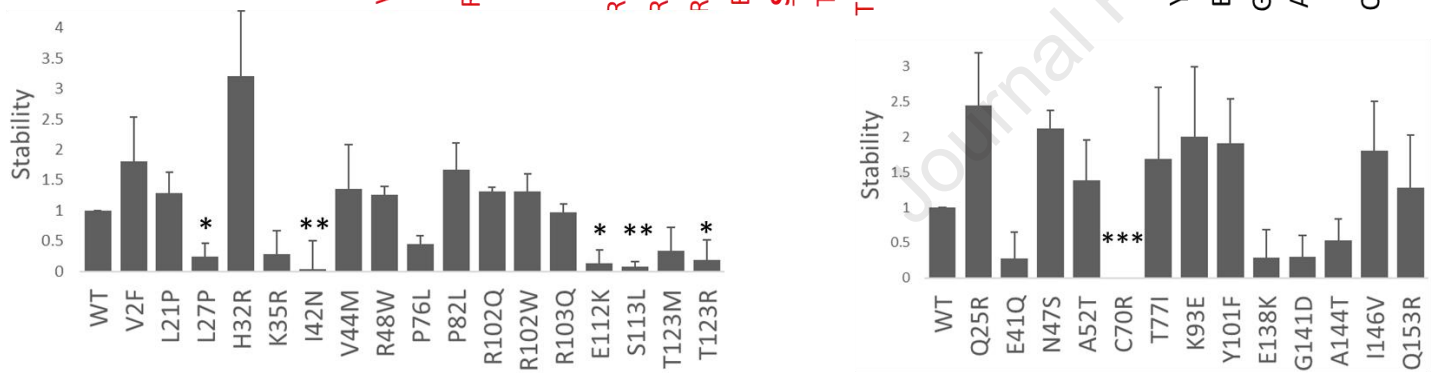

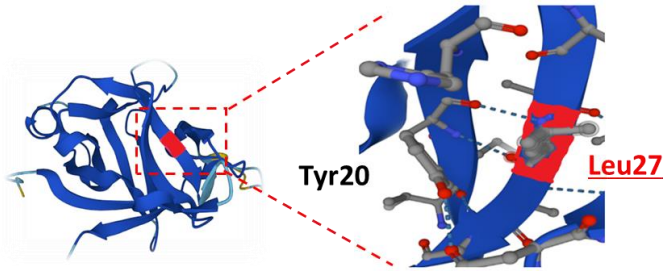

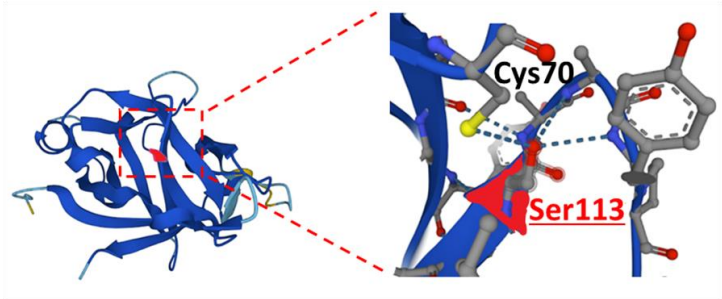

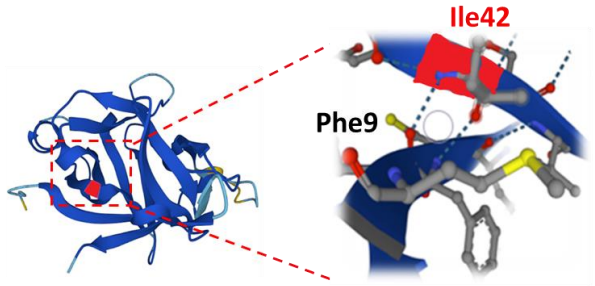

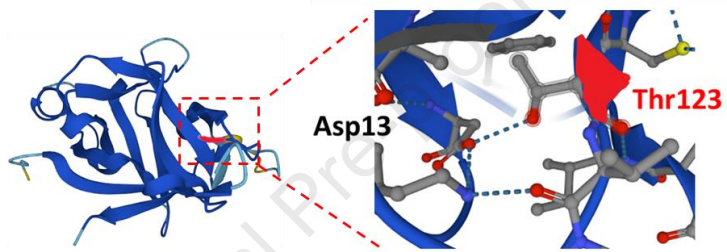

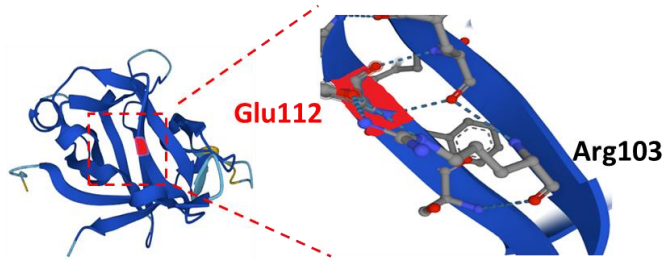

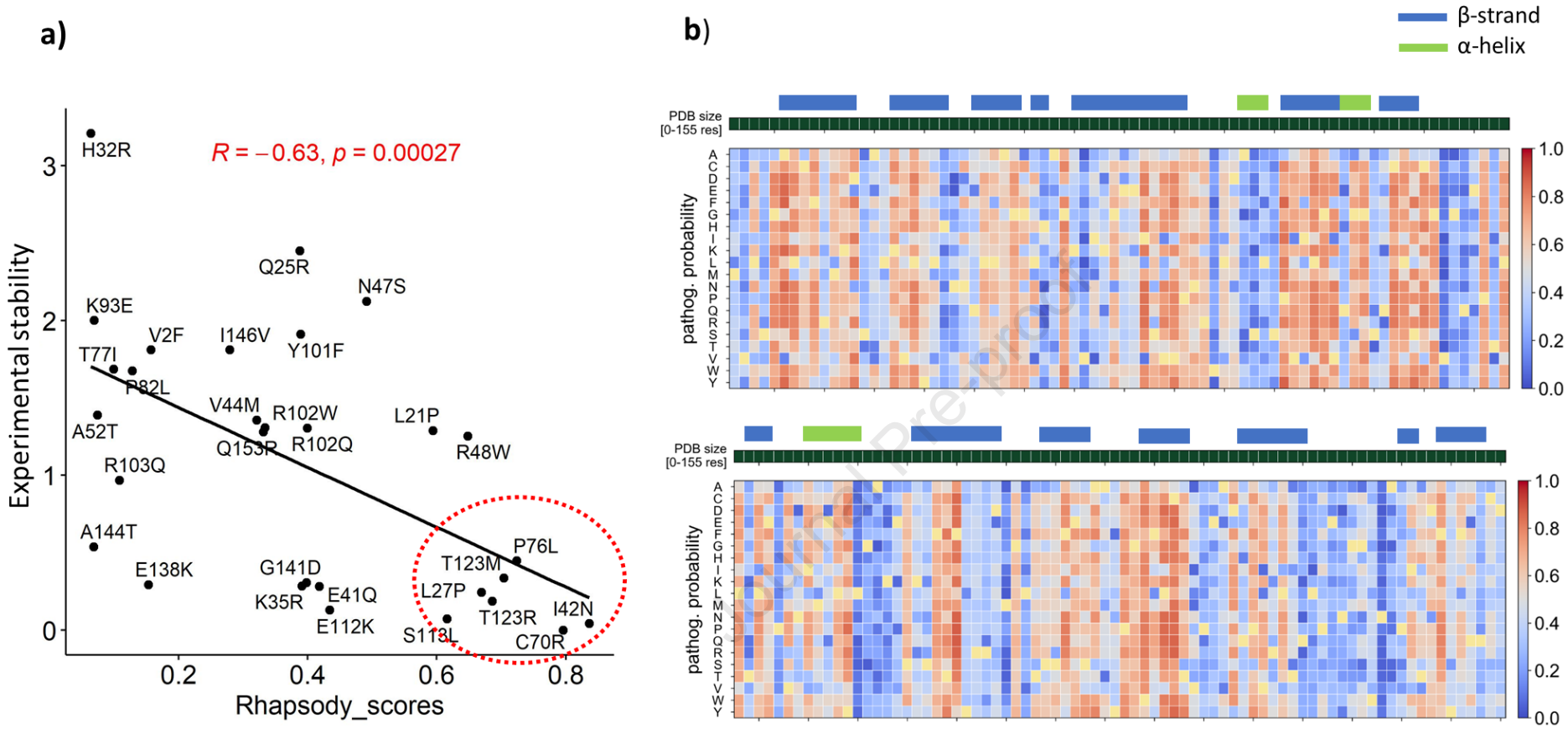
a)
R = −0.63, p = 0.00027
Experimental stability
Rhapsody_scores
H32R
Q25R
N47S
K93E
V2F
I146V
Y101F
T77I
P82L
V44M
R102W
L21P
A52T
Q153R
R102Q
R48W
R103Q
A144T
P76L
T123M
E138K
G141D
L27P
K35R
E41Q
T123R
I42N
E112K
S113L
C70R
b)
β-strand
α-helix
PDB size [0-155 res]
pathog. probability

a)

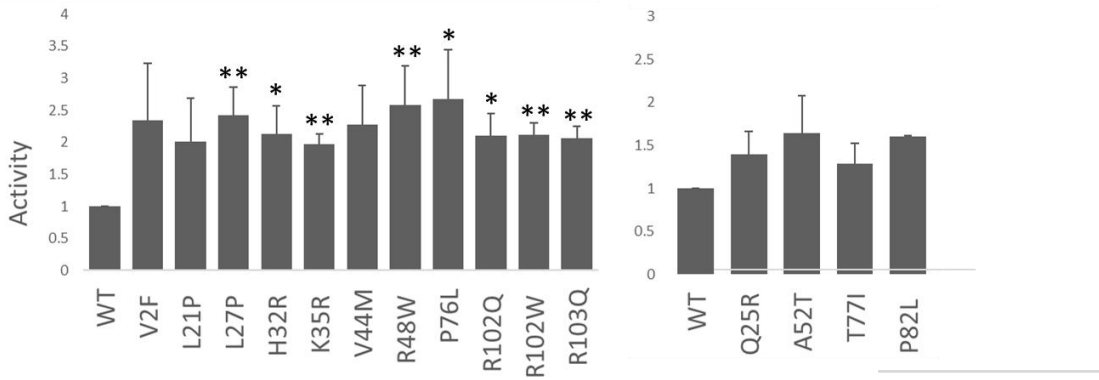

b)

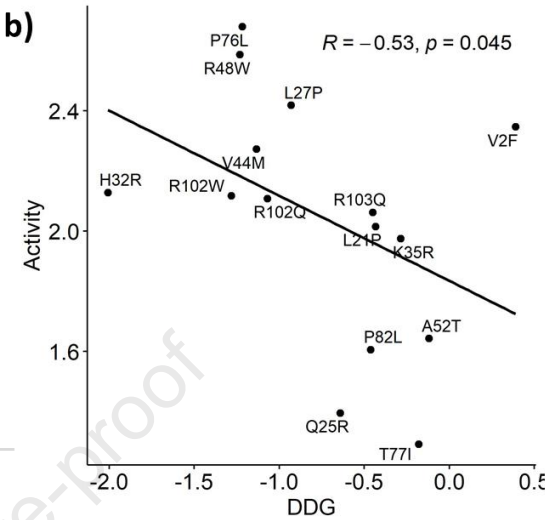

c)

M1	V2	L3	S4	G5	L7	C8	F9	R10	M11	K12	D13	S14	L16	K17	V18	L19	Y20	L21	H22	N23	N24	Q25	L26	L27	G29	G30	L31	H32	G34
-0.83	-0.30	-0.70	0.33	-0.20	-0.60	-0.77	-0.74	-0.43	-0.54	-0.33	-0.80	-0.45	-0.63	-0.25	-0.19	-0.53	-0.59	-0.21	-1.64	-1.56	-0.27	-0.60	-0.13	-0.68	-0.47	-0.05	-0.77	-0.98	-0.30

K35	V36	I37	K38	G39	E40	E41	I42	S43	V44	V45	P46	N47	R48	W49	L50	D51	S53	L54	S55	P56	V57	I58	L59	G60	V61	Q62	G63	G64	S65
-0.25	-0.21	-0.23	0.04	-0.36	-0.72	-0.36	-0.76	0.09	-0.62	0.04	-0.58	-0.33	-1.01	-0.90	-0.75	-0.29	-0.20	-0.50	-0.06	-0.43	-0.96	-0.13	-0.56	-0.77	-0.51	0.04	0.18	0.21	0.04

Q66	C67	L68	S69	C70	G71	V72	G73	Q74	E75	P76	T77	L78	T79	L80	E81	P82	V83	N84	I85	M86	E87	L88	Y89	L90	G91	K93	E94	S95	K96
-0.21	-0.73	-0.47	-0.13	-0.87	-0.14	0.31	-0.22	0.28	-0.39	-0.90	-0.25	-0.60	0.19	-0.35	-0.75	-0.54	-0.60	-0.02	-0.58	-0.71	-0.30	-0.53	-0.28	-0.44	-0.35	-0.08	-0.62	-0.15	-0.63

S97	F98	T99	F100	Y101	R102	R103	D104	M105	G106	L107	T108	S109	S110	F111	E112	S113	Y116	Y117	P117	G118	W119	F120	L121	T123	V124	P125	E126
0.00	-0.51	-0.39	-0.61	-0.57	-1.12	-0.40	-0.07	-0.78	-0.11	-0.28	-0.14	-0.28	-0.11	-0.80	-1.01	-0.06	-1.22	-1.17	-0.40	-0.19	-0.47	-0.40	-0.70	-0.10	-0.57	-0.49	-0.66

D128	Q129	P130	V131	R132	L133	T134	Q135	L136	P137	E138	N139	G140	G141	W142	N143	P145	I146	T147	D148	F149	Y150	F151	Q152	Q153	C154	D155
-0.45	-0.21	-0.07	-0.47	-0.59	-0.48	-0.30	-0.73	-0.64	-0.58	-0.23	-0.02	0.73	-0.26	-0.43	-0.71	-0.65	-0.68	-0.16	-0.20	-0.76	-0.59	-1.67	-1.11	-0.74	-0.87	0.20

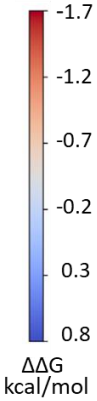

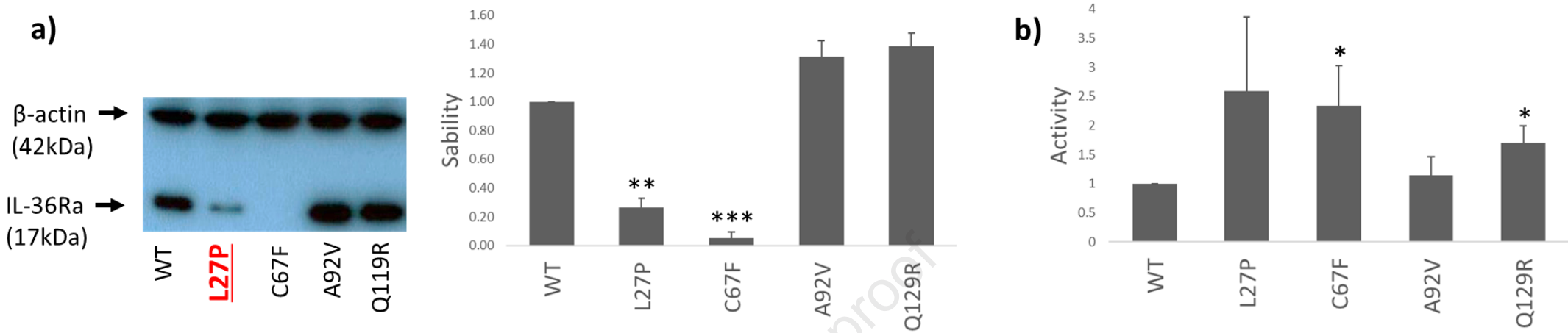

Supplemental Methods

Variant selection, pathogenicity predictions and evolutionary conservation analysis

dbSNP data (build 153) was accessed at https://www.ncbi.nlm.nih.gov/snp/. Pre-computed CADD scores were retrieved from the database hosted at cadd.gs.washington.edu, whereas GERP and REVEL scores were obtained through the Ensembl genome browser (www.ensembl.org). Rhapsody was accessed at http://rhapsody.csb.pitt.edu. The IL-36Ra PDB file (AF-Q9UBH0-F1-model_v3) retrieved from the AlphaFold2 database was used as an input for single-variant analysis and saturation mutagenesis.

Generation of mutagenized constructs

Constructs were generated using the QuikChange Lightning Site-Directed Mutagenesis Kit (Agilent Technologies, Santa Clara, CA; catalogue n. 210518) and primers designed with the QuikChange Primer Design tool (www.agilent.com/store/primerDesignProgram.jsp) (Table S5). Briefly, 10 ng wild-type construct was combined with 125ng of each primer, 5µl 10xQuickChange Lighting Buffer, 1µl dNTP Mix and 1.5µl QuickSolution reagent in a 50µl final volume. The reactions were incubated under the following cycling conditions: 2 min 95°C, 18x (20 sec 95°C, 10 sec 60°C, 2 min 68°C), 5 min 68°C. Next, the parental plasmid was digested with 2µl DpnI for 5 min at 37°C. Finally, the mutagenized plasmid was transformed into XL10-Gold ultracompetent cells and single-colonies were expanded. All constructs were validated by sequencing the entire *IL36RN* coding region, pCMV promoter, bovine growth hormone polyadenylation site and the myc sequence (Figure S3).

Cell culture

HEK293 cells were cultured in Dulbecco's Modified Eagle Medium (DMEM) supplemented with GlutaMax-I, 50U/ml of penicillin/50µg/ml of streptomycin and 10% Fetal Calf Serum (all from Life Technologies, Carlsbad, CA; catalogue n: 61965026, 15140122 and 10500064). HeLa-IL36R cells (kindly provided by Prof Seamus Martin, Trinity College Dublin, Ireland) were cultured in RPMI medium 1640 (Life Technologies; catalogue n: 21875034) supplemented as above.

Western blotting and ELISA

Cell lysates were loaded on a 15% polyacrylamide gel and electrophoresed for 2hr at 100V. Separated proteins were transferred to a PVDF membrane (Roche, Basel, Switzerland; catalogue n: 03010040001) and probed overnight at 4C with mouse anti c-myc (Santa Cruz Biotechnology, Dallas, TX; catalogue n: sc-40) and rabbit anti-β−actin (Cell Signalling Technology, Danvers, MA; catalogue n: 4967S) antibodies at a 1:1,000 dilution. The

membrane was then incubated for 1hr at room temperature with an HRP-conjugated secondary antibody (Polyclonal Anti-Mouse IgG (Agilent; catalogue n: P0447), or Polyclonal Anti-Rabbit IgG (GE Healthcare, Chicago, IL; catalogue n: NA934V)) diluted 1:10,000. Finally, the membrane was treated with the Amersham ECL Western Blotting Prime Detection Reagent (GE Healthcare; catalogue n: RPN2232) for 5 minutes. CL-Exposure autoradiography films (Thermo Fisher Scientific, Waltham, MA; catalogue n: 34090) were exposed to the membrane, developed using an automated film developer and analysed with ImageJ to measure IL-36Ra to β−actin ratios.

IL-8 levels were measured with the DuoSet CXCL8/IL-8 ELISA kit (RD Systems, Minneapolis, MN; catalogue n: DY208-05), using 1:40 dilutions of the culture supernatants.

Supplementary Figure Legends

Figure S1: Correlation between the experimental stability measurements reported in Figure 1c and the pathogenicity predictions obtained with CADD and REVEL. Each dot represents a mutant construct. The R value reported on top of each plot is the Spearman correlation coefficient.

Figure S2: Schematic representation of the IL-36Ra activity assay. HeLa-IL36R cells are treated with wild-type (left) or mutant (right) IL-36Ra protein. The wild-type protein binds IL-36R and limits the amount of IL-8 that is produced when cells are stimulated with IL-36 (left). The mutant protein cannot engage with IL-36R, so that IL-36 stimulation results in enhanced IL-8 production (right). Created with biorender.com

Figure S3: Chromatograms of mutagenized constructs for representative *IL36RN* changes, including patient (top panel) and population (bottom panel) variants.

Supplementary Tables

Table S1: Patient variants included in functional studies.

Table S2: Population variants included in functional studies.

Table S3: IL-36Ra residues that are most intolerant to substitutions.

Table S4: Features of the cytokines and chemokines that are upregulated by IL-36

Table S5: Sequence of mutagenesis primers

Table S1: Patient variants included in functional studies.

			Pathogenicity predictions		
Variant	*Frequency†*	*Reference*	*REVEL*	*CADD*	*Rhapsody*
p.Val2Phe	0.00005	(Bal et al., 2019)	0.15	25.2	0.16
p.Leu21Pro	0.00003	(Ellingford et al., 2016)	0.93	25.8	0.59
p.Leu27Pro	0.001	(Marrakchi et al., 2011)	0.60	24.3	0.67
p.His32Arg	-	(Körber et al., 2013)	0.15	21.4	0.06
p.Lys35Arg	0.001	(Setta-Kaffetzi et al., 2013)	0.42	23.3	0.39
p.Ile42Asn	0.000009	(Takeichi, 2017)	0.74	26.4	0.84
p.Val44Met	0.00006	(Wang et al., 2016)	0.17	18.7	0.32
p.Arg48Trp	0.001	(Onoufriadis et al., 2011)	0.63	25.6	0.65
p.Pro76Leu	0.005	(Körberet al., 2013)	0.58	23.0	0.72
p.Pro82Leu	0.004	(Li et al., 2014)	0.03	22.2	0.13
p.Arg102Trp	0.005	(Setta-Kaffetziet al., 2013)	0.58	23.1	0.33
p.Arg102Gln	0.000009	(Li et al., 2013)	0.42	25.1	0.40
p.Arg103Gln	0.00009	(Mossner et al., 2018)	0.09	22.2	0.11
p.Glu112Lys	0.00006	(Hayashi et al., 2014)	0.78	27.0	0.43
p.Ser113Leu	0.007	(Onoufriadiset al., 2011)	0.32	22.8	0.62
p.Thr123Arg	-	(Farooq et al., 2013)	0.62	23.5	0.69
p.Thr123Met	0.0001	(Kanazawa et al., 2013)	0.58	23.4	0.70

The recurrent p.Leu27Pro and p.Ser113Leu mutations are highlighted in bold font. †Maximum frequency observed across gnomAD (r2.1.1) populations.

Table S2: Population variants included in functional studies.

		Pathogenicity predictions			
Variant	*rs identifier*	*REVEL*	*CADD*	*Rhapsody*	*Frequency†*
p.Gln25Arg	rs867378394	0.43	23.3	0.39	-
p. Glu41Gln	rs771984756	0.42	24.7	0.42	0.00005
p.Asn47Ser	rs28938777	0.28	22.0	0.49	0.08
p.Ala52Thr	rs755465505	0.16	19.0	0.07	0.00005
p.Cys70Arg	rs375718709	0.79	23.7	0.80	0.00006
p.Thr77Ile	rs372880215	0.17	10.7	0.10	0.0001
p.Lys93Glu	rs746109701	0.08	6.5	0.07	0.00005
p.Tyr101Phe	rs769214649	0.39	18.4	0.39	0.0002
p.Glu138Lys	rs750580815	0.07	11.3	0.15	0.00003
p.Gly141Asp	rs758533837	0.09	0.7	0.40	0.00005
p.Ala144Thr	rs780261792	0.01	2.3	0.07	0.00003
p.Ile146Val	rs202059991	0.10	5.8	0.28	0.00009
p.Gln153Arg	rs771496493	0.26	4.8	0.33	0.00004

The common p.Asn47Ser variant is highlighted in bold font. †Maximum frequency observed across gnomAD (r2.1.1) populations.

Table S3: IL-36Ra residues that are most intolerant to substitutions.

Rhapsody stability analysis		*mCSM affinity analysis*	
Residue	*Pathogenicity score*[1]	*Residue*	*Pathogenicity score*[2]
Phe98	0.81	Phe151	-1.67 (C)
Phe100	0.78	His22	-1.64 (C)
Cys122	0.78	Asn23	-1.56 (C)
Val44	0.76	Tyr116	-1.22
Trp119	0.75	Cys122	-1.17
Leu59	0.75	Arg102	-1.12 (C)
Leu121	0.74	Gln152	-1.10 (C)
Cys67	0.74	Arg48	-1.01
Pro56	0.73	Glu112	-1.01
Leu19	0.72	His32	-0.98 (C)
Gly34	0.72	Val57	-0.96
Ala6	0.72	Pro76	-0.90
Pro117	0.71	Trp49	-0.90
Gly5	0.71	Cys154	-0.87 (C)
Gly60	0.71	Cys70	-0.87

[1]Average pathogenicity likelihood across all 19 possible substitutions; [2]ΔΔG measured by Ala scanning (kcal/mol); C, IL-36R/IL-36Ra contact residue.

Table S4: Features of the cytokines and chemokines that are upregulated by IL-36

	Fold up-regulation in primary keratinocytes treated with[1]			*Upregulated in GPP skin*[2]	*Downregulated by GPP treatment*	
	IL-36α	*IL-36β*	*IL-36γ*	-	*Skin*[3]	*Blood*[4]
IL36G	17.7	23.8	21.4	Yes	Yes	No
CXCL1	7.8	9.2	9.9	Yes	Yes	Yes
CCL20	7.6	9.0	9.2	Yes	No	No
CXCL8	**7.0**	**8.5**	**8.8**	**Yes**	**Yes**	**Yes**
IL32	5.6	5.7	5.6	No	No	Yes
IL1B	5.1	5.0	5.3	Yes	Yes	Yes
CXCL5	2.6	3.8	3.4	No	Yes	No
IL36RN	2.5	3.8	3.2	Yes	No	No
CXCL3	2.5	3.3	2.9	No	Yes	Yes
CXCL2	2.6	3.0	2.9	Yes	Yes	No
IL1A	2.8	2.3	2.5	No	No	No
IL24	2.6	2.2	2.6	No	Yes	No
IL23A	2.2	2.6	2.5	Yes	Yes	No
CXCL16	2.3	2.6	2.4	No	No	No
IL20	2.3	2.0	2.3	Yes	Yes	No

[1]Cultured keratinocytes (Mahil et al., 2017); [2]GPP vs healthy skin (Baum et al., 2022); [3]GPP skin sampled before and after treatment with spesolimab (Baum et al., 2022); [4]GPP peripheral blood mononuclear cells sampled before and after treatment with acitretin (Wang et al., 2018).

Table S5: Sequence of mutagenesis primers[1]

Variant	*Primers*
p.Val2Phe	CGCGATCGCCATGTTCCTGAGTGGGGC
	GCCCCACTCAGGAACATGGCGATCGCG
p.Leu21Pro	AGAAGCTGGTTATTATGCGGATAAAGCACCTTCAATGCC
	GGCATTGAAGGTGCTTTATCCGCATAATAACCAGCTTCT
p.Gln25Arg	GCCCTCCAGCTAGAAGCCGGTTATTATGCAGATAA
	TTATCTGCATAATAACCGGCTTCTAGCTGGAGGGC
p.Glu41Gln	GACCACGCTGATCTGTTCACCTTTAATGACCTTCCC
	GGGAAGGTCATTAAAGGTGAACAGATCAGCGTGGTC
p.Ile42Asn	GATTGGGGACCACGCTGTTCTCTTCACCTTTAATG
	CATTAAAGGTGAAGAGAACAGCGTGGTCCCCAATC
p.Val44Met	ACCGATTGGGGACCATGCTGATCTCTTCACC
	GGTGAAGAGATCAGCATGGTCCCCAATCGGT
p.Asn47Ser	CAGCCACCGACTGGGGACCACGCTGATC
	GATCAGCGTGGTCCCCAGTCGGTGGCTG
p.Arg48Trp	AGCGTGGTCCCCAATTGGTGGCTGGATGCCA
	TGGCATCCAGCCACCAATTGGGGACCACGCT
p.Ala52Thr	GGGACAGGCTGGTATCCAGCCACCGATTG
	CAATCGGTGGCTGGATACCAGCCTGTCCC
p.Cys67Phe	GGTGGAAGCCAGTTCCTGTCATGTGGG
	CCCACATGACAGGAACTGGCTTCCACC
p.Cys70Arg	GCCCCACCCCACGTGACAGGCACTG
	CAGTGCCTGTCACGTGGGGTGGGGC
p.Thr77Ile	GGTGGGGCAGGAGCCGATTCTAACACTAGAG
	CTCTAGTGTTAGAATCGGCTCCTGCCCCACC
p.Pro82Leu	GCTCCATGATGTTCACTAGCTCTAGTGTTAGAGTC
	GACTCTAACACTAGAGCTAGTGAACATCATGGAGC
p.Lys93Glu	GAAGCTCTTGGATTCCTCGGCACCAAGATAGAGCT
	AGCTCTATCTTGGTGCCGAGGAATCCAAGAGCTTC
p.Tyr101Phe	GTCCCGCCGGAAGAAGGTGAAGCTCTTGGA
	TCCAAGAGCTTCACCTTCTTCCGGCGGGAC
p.Arg102Gln	GCCCCATGTCCCGCTGGTAGAAGGTGAAG
	CTTCACCTTCTACCAGCGGGACATGGGGC
p.Arg103Gln	GAGCCCCATGTCCTGCCGGTAGAAGGT
	ACCTTCTACCGGCAGGACATGGGGCTC
p.Glu112Lys	GTAGGCAGCCGACTTGAAGCTGGAGGTGA
	TCACCTCCAGCTTCAAGTCGGCTGCCTAC
p.Ser113Leu	CCTCCAGCTTCGAGTTGGCTGCCTACCCGGG
	CCCGGGTAGGCAGCCAACTCGAAGCTGGAGG
p.Thr123Arg	GCTTCAGGCACCCTGCACAGGAACCAG
	CTGGTTCCTGTGCAGGGTGCCTGAAGC
p.Gln129Arg	CCTGAAGCCGATCGGCCTGTCAGACTCACCC
	GGGTGAGTCTGACAGGCCGATCGGCTTCAGG
p.Glu138Lys	CCAGCCACCATTCTTGGGAAGCTGGGTGA
	TCACCCAGCTTCCCAAGAATGGTGGCTGG
p.Gly141Asp	GGGGGCATTCCAGTCACCATTCTCGGG
	CCCGAGAATGGTGACTGGAATGCCCCC

p.Ala144Thr	CTGTGATGGGGGTATTCCAGCCACCATTCTCG
	CGAGAATGGTGGCTGGAATACCCCCATCACAG
p.Ile146Val	GGCTGGAATGCCCCCGTCACAGACTTCTACT
	AGTAGAAGTCTGTGACGGGGGCATTCCAGCC
p.Gln153Arg	GACTTCTACTTCCAGCGGTGTGACTAGGGCAAC
	GTTGCCCTAGTCACACCGCTGGAAGTAGAAGTC

[1] The p.Pro27Leu, p.His32Arg, p.Lys35Arg, p.Pro76Leu and p.Thr123Met constructs have been described elsewhere (Tauber et al., 2016)

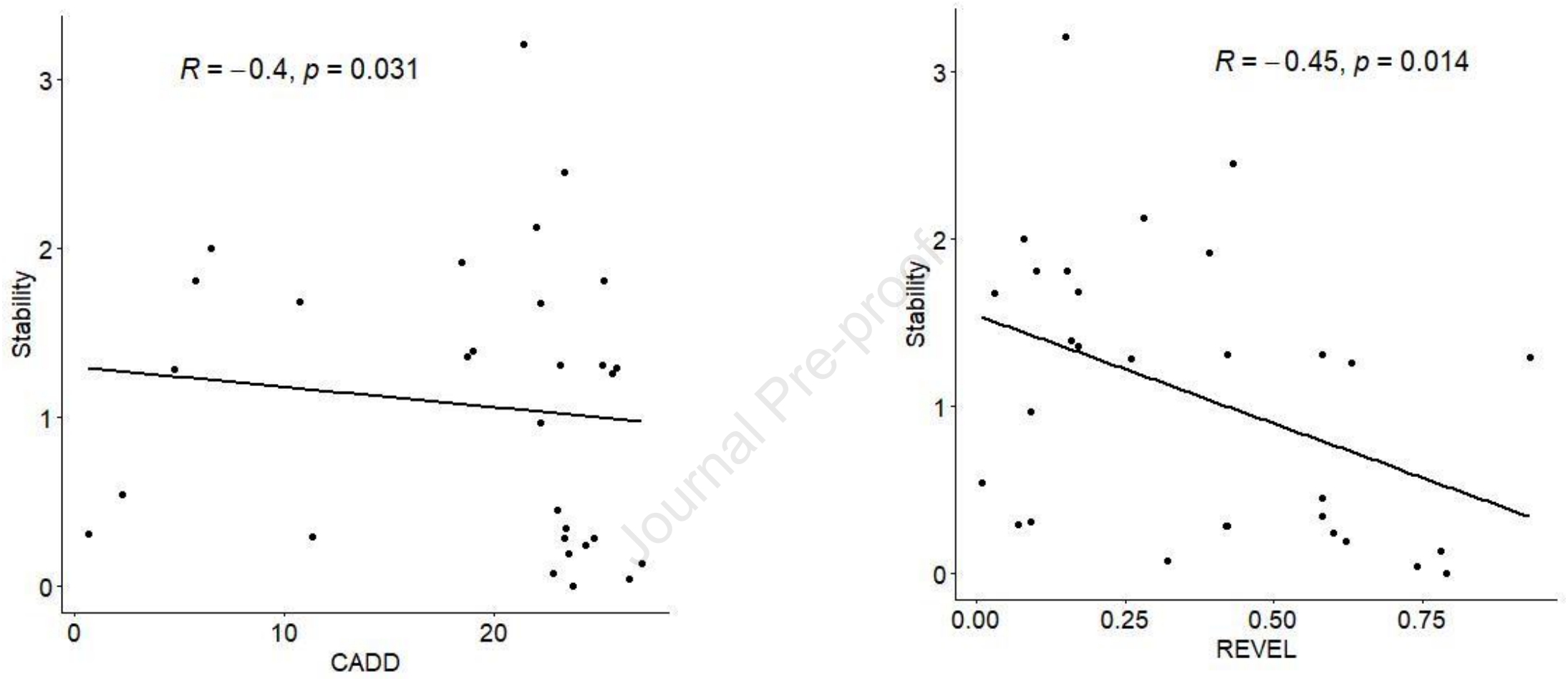

Figure S1: Correlation between the experimental stability measurements reported in Figure 1c and the pathogenicity predictions obtained with CADD and REVEL. Each dot represents a mutant construct. The R value reported on top of each plot is the Spearman correlation coefficient.

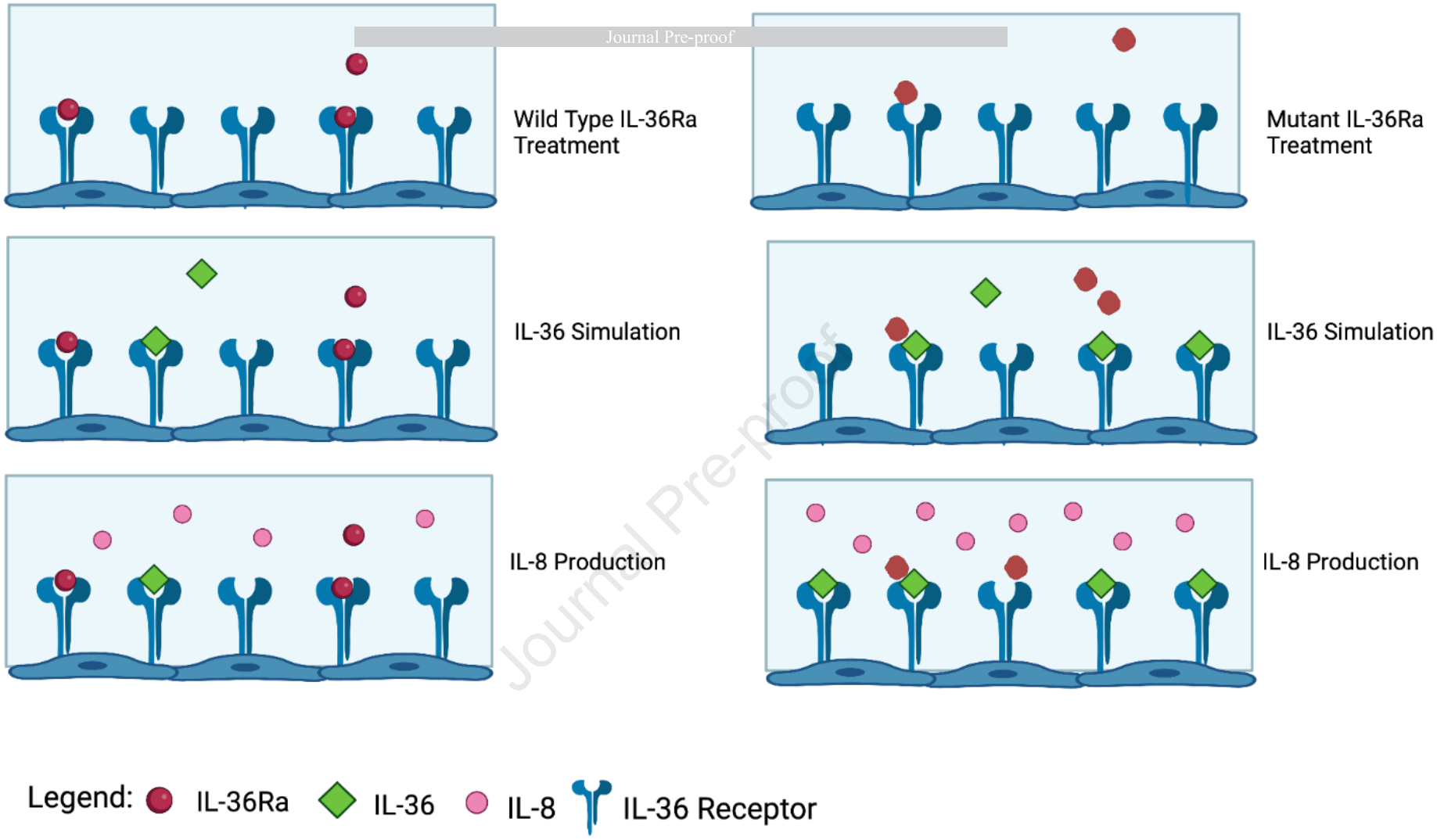

Figure S2: Schematic representation of the IL-36Ra activity assay. HeLa-IL36R cells are treated with wild-type (left) or mutant (right) IL-36Ra protein. The wild-type protein binds IL-36R and limits the amount of IL-8 that is produced when cells are stimulated with IL-36 (left). The mutant protein cannot engage with IL-36R, so that IL-36 stimulation results in enhanced IL-8 production (right). Created with biorender.com

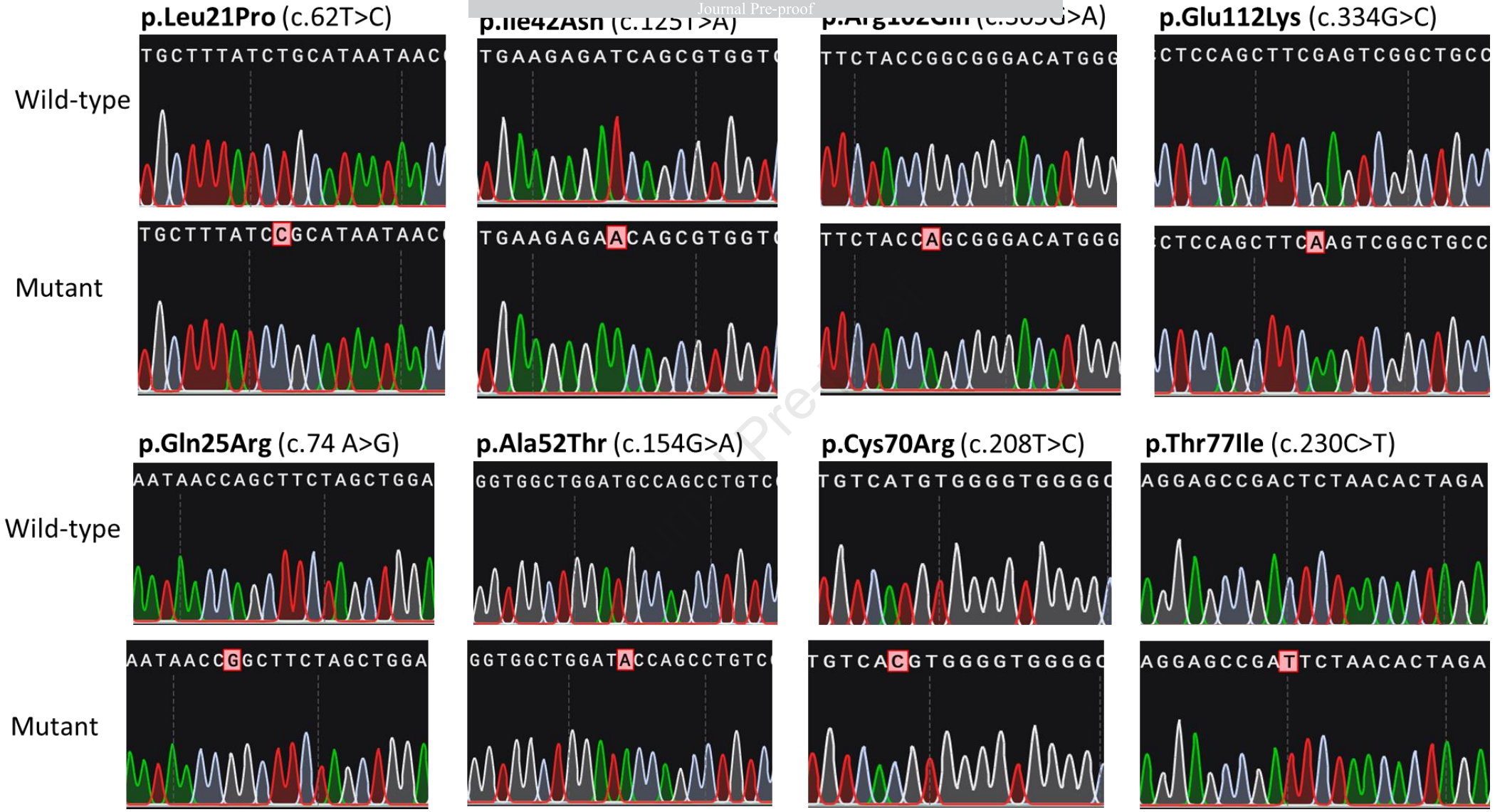

Figure S3: Chromatograms of mutagenized constructs for representative *IL36RN* changes, including patient (top panel) and population (bottom panel) variants.

Supplemental References

Bal E, Lim AC, Shen M, Douangpanya J, Madrange M, Gazah R, et al. Mutation in IL 36 RN impairs the processing and regulatory function of the interleukin-36-receptor antagonist and is associated with DITRA syndrome. Experimental dermatology 2019;28(10):1114-7.

Baum P, Visvanathan S, Garcet S, Roy J, Schmid R, Bossert S, et al. Pustular psoriasis: Molecular pathways and effects of spesolimab in generalized pustular psoriasis. The Journal of allergy and clinical immunology 2022;149(4):1402-12.

Ellingford J, Black G, Clayton T, Judge M, Griffiths C, Warren R. A novel mutation in IL 36 RN underpins childhood pustular dermatosis. Journal of the European Academy of Dermatology and Venereology 2016;30(2):302-5.

Farooq M, Nakai H, Fujimoto A, Fujikawa H, Matsuyama A, Kariya N, et al. Mutation analysis of the IL 36 RN gene in 14 Japanese patients with generalized pustular psoriasis. Human mutation 2013;34(1):176-83.

Hayashi M, Nakayama T, Hirota T, Saeki H, Nobeyama Y, Ito T, et al. Novel IL36RN gene mutation revealed by analysis of 8 Japanese patients with generalized pustular psoriasis. Journal of dermatological science 2014;76(3):267-9.

Kanazawa N, Nakamura T, Mikita N, Furukawa F. Novel IL36RN mutation in a Japanese case of early onset generalized pustular psoriasis. Journal of Dermatology 2013;40(9):749-51.

Körber A, Mössner R, Renner R, Sticht H, Wilsmann-Theis D, Schulz P, et al. Mutations in IL36RN in patients with generalized pustular psoriasis. The Journal of investigative dermatology 2013;133(11):2634.

Li M, Han J, Lu Z, Li H, Zhu K, Cheng R, et al. Prevalent and rare mutations in IL-36RN gene in Chinese patients with generalized pustular psoriasis and psoriasis vulgaris. The Journal of investigative dermatology 2013;133(11):2637-9.

Li XY, Chen MF, Fu X, Zhang QL, Wang ZZ, Yu GQ, et al. Mutation analysis of the IL36RN gene in Chinese patients with generalized pustular psoriasis with/without psoriasis vulgaris. Journal of Dermatological Science 2014;76(2):132-8.

Mahil SK, Catapano M, Di Meglio P, Dand N, Ahlfors H, Carr IM, et al. An analysis of IL-36 signature genes and individuals with IL1RL2 knockout mutations validates IL-36 as a psoriasis therapeutic target Science translational medicine 2017;9:eaan2514.

Marrakchi S, Guigue P, Renshaw BR, Puel A, Pei X-Y, Fraitag S, et al. Interleukin-36–receptor antagonist deficiency and generalized pustular psoriasis. New England Journal of Medicine 2011;365(7):620-8.

Mossner R, Wilsmann-Theis D, Oji V, Gkogkolou P, Lohr S, Schulz P, et al. The genetic basis for most patients with pustular skin disease remains elusive. British Journal of Dermatology 2018;178(3):740-8.

Onoufriadis A, Simpson MA, Pink AE, Di Meglio P, Smith CH, Pullabhatla V, et al. Mutations in IL36RN/IL1F5 are associated with the severe episodic inflammatory skin disease known as generalized pustular psoriasis. The American Journal of Human Genetics 2011;89(3):432-7.

Schneider CA, Rasband WS, Eliceiri KW. NIH Image to ImageJ: 25 years of image analysis. Nature methods 2012;9(7):671-5.

Setta-Kaffetzi N, Navarini AA, Patel VM, Pullabhatla V, Pink AE, Choon S-E, et al. Rare pathogenic variants in IL36RN underlie a spectrum of psoriasis-associated pustular phenotypes. The Journal of investigative dermatology 2013;133(5):1366-9.

Takeichi T. A newly revealed IL36RN mutation in sibling cases complements our IL36RN mutation statistics for generalized pustular psoriasis. Department of Dermatology, Fujita Health University; 2017.

Tauber M, Bal E, Pei XY, Madrange M, Khelil A, Sahel H, et al. IL36RN Mutations Affect Protein Expression and Function: A Basis for Genotype-Phenotype Correlation in Pustular Diseases. J Invest Dermatol 2016;136(9):1811-9.

Wang L, Yu X, Wu C, Zhu T, Wang W, Zheng X, et al. RNA sequencing-based longitudinal transcriptomic profiling gives novel insights into the disease mechanism of generalized pustular psoriasis. BMC Med Genomics 2018;11(1):52.

Wang T-S, Chiu H-Y, Hong J-B, Chan C-C, Lin S-J, Tsai T-F. Correlation of IL36RN mutation with different clinical features of pustular psoriasis in Chinese patients. Archives of dermatological research 2016;308(1):55-63.